International Journal of Multiphase Flow 39 (2012) 78–87

Contents lists available at SciVerse ScienceDirect

International Journal of Multiphase Flow

journal homepage: www.elsevier.com/locate/ijmulflow

Effects of surfactant on terminal velocity of a Taylor bubble in a vertical pipe

Kosuke Hayashi *, Akio Tomiyama

Graduate School of Engineering, Kobe University, 1-1, Rokkodai, Nada, Kobe 657-8501, Japan

ARTICLE INFO

Article history:
Received 30 August 2011
Received in revised form 4 November 2011
Accepted 6 November 2011
Available online 12 November 2011

Keywords:
Taylor bubble
Surfactant
Adsorption
Desorption
Interface tracking method

ABSTRACT

Effects of soluble surfactant on the terminal velocity of a Taylor bubble rising through a vertical pipe are investigated using an interface tracking method. A level set method is utilized to track the interface. Transport of surfactant in the bulk liquid and at the interface is taken into account. The amount of adsorption and desorption is evaluated using the Frumkin and Levich model. The normal component of surface tension force is computed using a ghost fluid method, whereas the tangential component, i.e., the Marangoni force, is evaluated by making use of the continuum surface force model. Simulations of small air bubbles contaminated with soluble surfactant are carried out for validation. The Marangoni effects on the bubbles, i.e., the surface immobilization and the increase in drag coefficient, are well predicted. Then Taylor bubbles rising through vertical pipes filled with contaminated water at a low Morton number are simulated for various Eötvös numbers, various bulk surfactant concentrations and two different surfactants, i.e., 1-pentanol and Triton X-100. As a result, the following conclusions are obtained: (1) the reduction of surface tension near the bubble nose is the cause of the increase in terminal velocity, (2) the surfactant does not affect the terminal velocities of high Eötvös number bubbles since the bubbles at high Eötvös numbers are independent of surface tension, (3) the terminal velocity of a low Morton number Taylor bubble can be evaluated by making use of available correlations for clean Taylor bubbles, provided that the degree of contamination near the bubble nose is known and the Marangoni effect in the nose region is negligible, and (4) the Hatta number, which is the ratio of the adsorption velocity to the bubble velocity, is a primary factor governing the degree of contamination in the bubble nose region.

1. Introduction

Slug flow is one of the typical two-phase flow patterns encountered in various industrial applications. The flow is characterized by the presence of large bullet-shaped bubbles, which are called Taylor bubbles.

If a Taylor bubble in a vertical pipe filled with a stagnant liquid is free from a surface-active agent (surfactant), the force balance between the inertial, viscous, surface tension and buoyant forces determines the bubble motion. These forces give three independent dimensionless groups governing the bubble motion, e.g., the Froude number, $\mathrm{Fr} = V_T/\sqrt{\Delta\rho g D/\rho_L}$, the Eötvös number, $\mathrm{Eo}_D = \Delta\rho g D^2/\sigma_0$, and the Morton number, $M = \mu_L{}^4\Delta\rho g/\rho_L{}^2\sigma_0{}^3$, where V_T is the bubble terminal velocity, $\Delta\rho$ the density difference between the two phases, g the magnitude of the acceleration of gravity, D the pipe diameter, ρ the density, σ_0 the surface tension of the clean surface, μ the viscosity, and the subscript L denotes the continuous liquid phase. A number of studies on the Froude number of the clean Taylor bubble have been carried out and several correlations of Fr applicable to a wide range of M and Eo_D have been proposed, e.g., Wallis (1969), Viana et al. (2003) and Hayashi et al. (2010). On the other hand, our knowledge on the motion of a Taylor bubble contaminated with surfactant is still insufficient and no Froude number models have been proposed for contaminated Taylor bubbles.

Almatroushi and Borhan (2004) measured terminal velocities of Taylor bubbles in glycerol–water solutions contaminated with sodium dodecyl sulfate at low Reynolds numbers and for $12 \leqslant \Delta\rho g D^2/\sigma_c \leqslant 26$, where σ_c is the surface tension at the critical micelle concentration. They pointed out that the presence of surfactant increases V_T of the Taylor bubbles, and speculated that the cause of the increase in V_T is the reduction in surface tension due to the surfactant adsorption and the surface immobilization due to the Marangoni effect is weak since large shape deformation dilutes the surfactant concentration at the surface. To the contrary, it is well known that the terminal velocities of Taylor bubbles at high Eo_D numbers and low M numbers are independent of the presence of surfactant. Detailed investigation of these surfactant effects may reveal a key physics in developing the Froude number model for contaminated Taylor bubbles.

Interface tracking methods are useful tools for investigating the motion of a contaminated bubble, since they may be able to

* Corresponding author. Tel./fax: +81 78 803 6108.
E-mail addresses: hayashi@mech.kobe-u.ac.jp (K. Hayashi), tomiyama@mech.kobe-u.ac.jp (A. Tomiyama).

0301-9322/$ - see front matter © 2011 Elsevier Ltd. All rights reserved.
doi:10.1016/j.ijmultiphaseflow.2011.11.001

consider all the surfactant dynamics, i.e., the advection and diffusion of surfactant in the bulk liquid and at the bubble surface and the adsorption–desorption kinetics.

Several interface tracking methods for simulating motions of bubbles contaminated with soluble surfactant have been proposed. Cuenot et al. (1997) carried out simulations of spherical bubbles using a boundary-fitted coordinate (BFC) method. The adsorption and desorption were taken into account by using the Frumkin and Levich model (Frumkin and Levich, 1947; Levich, 1962). Liao and McLaughlin (2000) investigated the motions of small bubbles contaminated with decanoic acid by using a BFC method. Takagi et al. (2003) carried out experiments on nitrogen bubbles in water contaminated with three different surfactants, i.e., 1-pentanol, 3-pentanol and Triton X-100, and BFC simulations of spherical bubbles under the same conditions as the experiments. The simulation confirmed that the surfactant distribution at the interface and the interfacial velocity strongly depend on the adsorption and desorption properties of surfactant. Only two-dimensional axisymmetric bubbles were dealt with in the above studies. Fukuta et al. (2008) and Takagi et al. (2009) carried out three-dimensional BFC simulations of contaminated spherical bubbles in linear shear flows to investigate the effects of surfactant on the lift force. These BFC methods did not solve the flows inside bubbles. On the other hand, Tukovic and Jasak (2008) developed a three-dimensional BFC method solving the flows both inside and outside a bubble. A front tracking method for simulating bubbles contaminated with soluble surfactant was proposed by Muradoglu & Tryggvason (2008). They validated their method through several benchmark tests, e.g., a spherical bubble expanding at a constant speed, bubble migration due to the Marangoni force, and free rising bubbles in contaminated liquids at low Reynolds numbers. As for an Eulerian approach, Alke and Bothe (2009) proposed a volume-of-fluid (VOF) method for simulating contaminated bubbles. They simulated a spheroidal bubble in a vertical pipe and obtained a surfactant distribution corresponding to a stagnant cap model.

Only spherical or slightly deformed bubbles were dealt with in the above studies, and there are no studies on the detailed surfactant motion on bubbles with large shape deformation such as Taylor bubbles.

In this study, an interface tracking method is, therefore, developed to predict the motions of contaminated Taylor bubbles. The Eulerian approach may be suitable for bubbles with large shape deformation. A level set method is, therefore, utilized for tracking the interface. An extrapolation method proposed by Xu and Zhao (2003) is adopted to facilitate the evaluation of the surface gradient of the surface surfactant concentration on Eulerian grids. The adsorption–desorption kinetics is accounted for by using the Frumkin–Levich model. The developed method will be validated through simulations of small air bubbles rising through stagnant water contaminated with soluble surfactant. Then effects of surfactant on Taylor bubble shape and velocity will be investigated for a wide range of Eo_D. This study focuses on Taylor bubbles in a low Morton number system.

2. Field equations

The continuity and momentum equations for incompressible Newtonian fluids based on the one-fluid formulation are given by:

$$\nabla \cdot \boldsymbol{V} = 0 \tag{1}$$

$$\frac{\partial \boldsymbol{V}}{\partial t} + \boldsymbol{V} \cdot \nabla \boldsymbol{V} = -\frac{1}{\rho}\nabla P + \frac{1}{\rho}\nabla \cdot \mu\left[\nabla \boldsymbol{V} + (\nabla \boldsymbol{V})^T\right] + \boldsymbol{g} + \frac{1}{\rho}[\sigma\kappa\boldsymbol{n} + \nabla_S\sigma]\delta \tag{2}$$

where $\boldsymbol{V}$ is the velocity, t the time, P the pressure, $\boldsymbol{g}$ the acceleration of gravity, σ the surface tension, κ the curvature, $\boldsymbol{n}$ the unit normal to the interface, ∇_S ($=\nabla - \boldsymbol{nn}\cdot\nabla$) the surface gradient operator, δ the delta function, which is non-zero only at the interface, and the superscript T denotes the transpose. The last term, $(\nabla_S\sigma)\delta$, is the surface tension force tangent to the interface and is the cause of the Marangoni effect. The transport equation of surfactant in the continuous phase and that at the interface are given by (Levich, 1962; Stone, 1990; Cuenot et al., 1997)

$$\frac{\partial C}{\partial t} + \boldsymbol{V} \cdot \nabla C = \nabla \cdot D_C \nabla C \tag{3}$$

$$\frac{\partial \Gamma}{\partial t} + \nabla_S \cdot \Gamma \boldsymbol{V}_S = \nabla_S \cdot D_S \nabla_S \Gamma + \dot{S}_\Gamma \tag{4}$$

where C is the surfactant concentration in the continuous phase, Γ the surfactant concentration at the interface, D_C and D_S are the diffusion coefficient in the continuous phase and that at the interface, respectively, and $\boldsymbol{V}_S$ the tangential component of $\boldsymbol{V}$. The source term $\dot{S}_\Gamma$ is the molar flux from the continuous phase to the interface due to the adsorption and desorption, i.e., $\dot{S}_\Gamma = -D_C(\boldsymbol{n}\cdot\nabla C|_{int})$, and is evaluated by using the Frumkin and Levich model (Frumkin and Levich, 1947; Levich, 1962):

$$\dot{S}_\Gamma = k[C_S(\Gamma_{\max} - \Gamma) - \beta\Gamma] \tag{5}$$

where k and β are parameters for the adsorption and desorption kinetics, respectively, $\Gamma_{\max}$ the saturation value of Γ, and C_S the molar concentration of the continuous phase in the vicinity of the interface.

The interface is tracked by solving the following level set equation (Sussman et al., 1994):

$$\frac{\partial \phi}{\partial t} + \boldsymbol{V} \cdot \nabla \phi = 0 \tag{6}$$

where ϕ is the level set function, and the interface is given by the zero-level set, $\phi = 0$. The unit normal and the curvature are given by:

$$\boldsymbol{n} = \frac{\nabla \phi}{|\nabla \phi|} \tag{7}$$

$$\kappa = -\nabla \cdot \frac{\nabla \phi}{|\nabla \phi|} \tag{8}$$

3. Numerical method

3.1. Method for solving continuity and momentum equations

Several methods for evaluating the normal component of the surface tension force, $\sigma\kappa\delta\boldsymbol{n}$, are available, e.g., the continuum surface tension force (CSF) model (Brackbill et al., 1992), the ghost fluid method (GFM) (Kang et al., 2000) and the immersed interface method (IIM) (LeVeque and Li, 1994). The IIM is the most accurate but not computationally efficient because of the necessity of jump conditions for high order derivatives of physical quantities. On the other hand the CSF model is the simplest but causes large spurious currents. The simplicity and accuracy of the GFM are in-between. The GFM is adopted to evaluate the normal component of the surface tension force in this study.

The momentum equation without the pressure gradient and the normal component of surface tension force is solved to obtain a temporary velocity, $\boldsymbol{V}^*$, for the velocity:

$$\boldsymbol{V}^* = \boldsymbol{V}^n + \Delta t\left[-\boldsymbol{V}\cdot\nabla\boldsymbol{V} + \frac{1}{\rho}\nabla\cdot\mu\left[\nabla\boldsymbol{V} + (\nabla\boldsymbol{V})^T\right] + \boldsymbol{g} + \frac{(\nabla_S\sigma)\delta}{\rho}\right]^n \tag{9}$$

where the superscript n denotes the time step and Δt is the time step size, i.e., $t = n\Delta t$. The advection and diffusion terms in Eq. (9) are evaluated by using the cubic interpolated propagation (CIP) scheme (Takewaki and Yabe, 1987) and the second-order centered-difference scheme, respectively. The density ρ and viscosity μ are given by

$$\rho = \rho_D + (\rho_C - \rho_D)H_\varepsilon(\phi) \tag{10}$$

$$\mu = \mu_D + (\mu_C - \mu_D)H_\varepsilon(\phi) \tag{11}$$

where the subscripts D and C denote the dispersed and continuous phases, respectively, and $H_\varepsilon(\phi)$ is the smoothed Heaviside function given by:

$$H_\varepsilon(\phi) = \begin{cases} 0 & \phi < -\varepsilon \\ \frac{1}{2} + \frac{\phi}{2\varepsilon} + \frac{1}{2\pi}\sin\left(\frac{\pi\phi}{\varepsilon}\right) & |\phi| \leqslant \varepsilon \\ 1 & \phi > \varepsilon \end{cases} \tag{12}$$

Here the parameter ε is set at $1.5\Delta x$, where Δx is the cell size. It has been pointed out that the harmonic mean, $\mu^{-1} = \mu_C^{-1}H_\varepsilon + \mu_D^{-1}(1 - H_\varepsilon)$, of the viscosity is more accurate than the arithmetic mean, Eq. (11) (Prosperetti, 2002; Tryggvason et al., 2011). It should, however, be noted that the harmonic mean is derived from the continuity of the tangential viscous stress at the interface but the viscous stress possesses the jump caused by the Marangoni force at contaminated interfaces. Hence the harmonic mean does not give the correct tangential component of the momentum jump condition when $\nabla_S\sigma \neq 0$. This will be demonstrated in Section 4.1.

The CSF model is utilized to evaluate the Marangoni force, $(\nabla_S\sigma)\delta$, because of its simplicity:

$$(\nabla_S\sigma)\delta = \left[\nabla\sigma - \frac{\nabla\phi}{|\nabla\phi|}\left(\frac{\nabla\phi}{|\nabla\phi|}\cdot\nabla\sigma\right)\right]\left(\frac{2\rho}{\rho_D + \rho_C}\right)\delta_\varepsilon(\phi) \tag{13}$$

where $\delta_\varepsilon(\phi)$ is the smoothed delta function given by:

$$\delta_\varepsilon(\phi) = \begin{cases} \frac{1}{2\varepsilon}\left[1 + \cos\left(\frac{\pi\phi}{\varepsilon}\right)\right] & |\phi| < \varepsilon \\ 0 & \text{otherwise} \end{cases} \tag{14}$$

The pressure at the new time step $n + 1$ is obtained by solving the following Poisson equation:

$$\nabla\cdot\frac{\Delta t}{\rho}\nabla P^{n+1} = \nabla\cdot\boldsymbol{V}^* \tag{15}$$

When evaluating the pressure gradient in the above equation, the normal component of surface tension force is accounted for. Let us consider the following case: the center of the cell i belongs to the phase D and that of the neighboring cell, $i + 1$, in the x direction belongs to the phase C. In this case, the term, $(1/\rho)\partial P/\partial x|_{i+1/2}$, at the cell face $i + 1/2$ is evaluated as

$$\left.\frac{1}{\rho}\frac{\partial P^{n+1}}{\partial x}\right|_{i+1/2} = \frac{1}{\rho^*}\frac{P_{i+1}^{n+1} - P_i^{n+1}}{\Delta x} - \frac{1}{\rho^*}\frac{[P]_{int}}{\Delta x} \tag{16}$$

where ρ^* is given by:

$$\rho^* = \theta\rho_D + (1 - \theta)\rho_C \tag{17}$$

and the fraction θ is:

$$\theta = \frac{|\phi_i|}{|\phi_i| + |\phi_{i+1}|} \tag{18}$$

The second term in Eq. (16) expresses the contribution of the jump in P due to the surface tension force in the normal direction, i.e.:

$$[P]_{int} = \sigma\kappa \tag{19}$$

If the cells, i and $i + 1$, belong to the continuous and dispersed phases, respectively, the following equations are used instead of Eqs. (16) and (17):

$$\left.\frac{1}{\rho}\frac{\partial P^{n+1}}{\partial x}\right|_{i+1/2} = \frac{1}{\rho^*}\frac{P_{i+1}^{n+1} - P_i^{n+1}}{\Delta x} + \frac{1}{\rho^*}\frac{[P]_{int}}{\Delta x} \tag{20}$$

$$\rho^* = \theta\rho_C + (1 - \theta)\rho_D \tag{21}$$

Then $\boldsymbol{V}^*$ is projected onto the divergence-free vector $\boldsymbol{V}^{n+1}$:

$$\boldsymbol{V}^{n+1} = \boldsymbol{V}^* - \frac{\Delta t}{\rho}\nabla P^{n+1} \tag{22}$$

The pressure gradient in the above equation is evaluated in the same way as in Eqs. (16) and (20).

3.2. Level set method

The level set equation, Eq. (6), is solved by using the 5th-order weighted essentially non-oscillatory (WENO) scheme and the 3rd-order Runge–Kutta scheme (Fedkiw et al., 1999). The level set function will not be a distance function after advecting ϕ. The following re-initialization equation is, therefore, solved at each time step to recover the property of ϕ as the distance function (Sussman et al., 1994):

$$\frac{\partial\phi}{\partial\tau} = sign(\phi)[1 - |\nabla\phi|] \tag{23}$$

where τ is the pseudo time and sign(ϕ) the sign function given by:

$$sign(\phi) = \frac{\phi}{\sqrt{\phi^2 + \Delta x^2}} \tag{24}$$

The WENO and Runge–Kutta schemes are also used to solve Eq. (23).

As is well known, the re-initialization slightly changes the interface position, and therefore, the mass conservation is deteriorated. Several methods for preserving the fluid volume, therefore, have been proposed, e.g., Chang et al. (1996), Meier (2000), Sussman et al. (1998) and Enright et al. (2002). Meier's global correction method is utilized in this study. The level set function, ϕ^*, after solving Eq. (23) is updated by using the following equation:

$$\phi^{n+1} = \phi^* + \frac{\sum[H_\varepsilon(\phi(t=0))\Delta\Theta - H_\varepsilon(\phi^*)\Delta\Theta]}{\sum\delta(\phi^*)\Delta\Theta} \tag{25}$$

where $\Delta\Theta$ is the cell volume and the summation is taken for all the computational cells.

3.3. Transport equations of C and Γ

Eq. (3) is solved using the method proposed by Muradoglu and Tryggvason (2008). Instead of dealing with the correct boundary condition, $\dot{S}_\Gamma = -D_C(\boldsymbol{n}\cdot\nabla C|_{int})$, $\dot{S}_\Gamma$ is dealt with as an interfacial source term, i.e.

$$\frac{\partial C}{\partial t} + \boldsymbol{V}\cdot\nabla C = \nabla\cdot D_C\nabla C - \dot{S}_\Gamma\delta(\phi), \tag{26}$$

and this equation is solved under the boundary condition, $\boldsymbol{n}\cdot\nabla C|_{int} = 0$. This numerical method gives a sort of approximate solutions to Eq. (3) and $\dot{S}_\Gamma = -D_C(\boldsymbol{n}\cdot\nabla C|_{int})$. Hence its validity should be examined through comparisons with available data.

The surfactant never exists inside the dispersed phase. The surfactant concentration inside the dispersed phase, therefore, has no effects on the result of numerical simulation but can be used only to satisfy the boundary condition, $\boldsymbol{n}\cdot\nabla C|_{int} = 0$, in finite difference calculations. The concentration in the dispersed phase is given as

the solution in the steady state of the following equation (Aslam, 2003):

$$\frac{\partial C}{\partial \tau} + \mathrm{sign}(\phi)\mathbf{n}\cdot\nabla C = 0 \tag{27}$$

This equation extrapolates the value of C at the interface into the dispersed phase, and the solution in the steady state, $\partial C/\partial\tau = 0$, satisfies $\mathrm{sign}(\phi)\boldsymbol{n}\cdot\nabla C = 0$.

The molar concentration Γ at the interface is extrapolated into both phases by solving the following equation (Xu and Zhao, 2003):

$$\frac{\partial \Gamma}{\partial \tau} + sign(\phi)\mathbf{n}\cdot\nabla\Gamma = 0 \tag{28}$$

The extrapolated Γ satisfies:

$$\mathbf{n}\cdot\nabla\Gamma = 0 \tag{29}$$

in the two phases and at the interface. Hence $\nabla_S\Gamma = \nabla\Gamma - \boldsymbol{nn}\cdot\nabla\Gamma = \nabla\Gamma$. Once Γ is extrapolated, the transport equation of Γ can be solved with any difference schemes. When solving Eq. (4), it is transformed to the following form (Xu and Zhao, 2003; James and Lowengrub, 2004; Xu et al., 2006):

$$\frac{\partial \Gamma}{\partial t} + \mathbf{V}\cdot\nabla\Gamma = D_S\left(\nabla\cdot\nabla\Gamma - \frac{\partial^2\Gamma}{\partial n^2} + \kappa\frac{\partial\Gamma}{\partial n}\right) + (\mathbf{n}\cdot\nabla\mathbf{V}\cdot\mathbf{n})\Gamma + \dot{S}_\Gamma \tag{30}$$

The advection and diffusion terms in Eqs. (26) and (30) are discretized by using the WENO and Runge–Kutta schemes, whereas the second-order ENO scheme is adopted to the extrapolation equations, Eqs. (27) and (28). Eqs. (27), (28), and (30) are solved only in the vicinity of the interface.

The surface tension σ is calculated using:

$$\sigma(\Gamma) = \sigma_0\left[1 + \frac{R_G T\Gamma_{max}}{\sigma_0}\ln\left(1 - \frac{\Gamma}{\Gamma_{max}}\right)\right] \tag{31}$$

where R_G is the universal gas constant and T the temperature (Frumkin and Levich, 1947).

4. Results and discussion

4.1. Small air bubbles rising through stagnant water

Air bubbles rising through stagnant water contaminated with surfactant are simulated to examine whether or not the proposed method gives accurate predictions for the Marangoni effects on the bubbles. The range of the sphere-volume equivalent bubble diameter, d, is from 0.60 to 0.98 mm. These bubbles rise rectilinearly (Aybers and Tapucu, 1969) and their shapes are axisymmetric. Therefore the flow is assumed to be axisymmetric and the two-dimensional cylindrical coordinates (r,z) are used.

Fig. 1 shows the computational domain. The left boundary is the axis of symmetry. The uniform velocity, $-V_B(t)$, is imposed on the top, bottom and right boundaries, where $V_B(t)$ is the instantaneous bubble velocity. The instantaneous acceleration of the bubble with the opposite sign is added to Eq. (2) to fix the bubble position (Wang et al., 2008). The dimensions of the domain in the r and z directions are $8d$ and $16d$, respectively. Since the ratio of the bubble radius to $8d$ is much smaller than 0.125, the bubble can be regarded as being in infinite water (Clift et al., 1978). The number of cells assigned to the bubble diameter is 48. Uniform square cells are used near the bubble, whereas non-uniform coarser cells are used for the other region.

The fluid properties of two phases are those for air and water at room temperature and atmospheric pressure. The adsorption and desorption properties of 1-pentanol are used, i.e., $k = 5.08\ \mathrm{m^3/mol\,s}$, $\beta = 21.7\ \mathrm{mol/m^3}$ and $\Gamma_{\max} = 5.9\times10^{-6}\ \mathrm{mol/m^2}$ (Takagi et al., 2003). The diffusion coefficient, D_C, in the bulk liquid is $1.1\times10^{-9}\ \mathrm{m^2/s}$ and it is assumed that $D_C = D_S$ (Takagi et al., 2009). The initial value, C_∞, of the bulk concentration ranges from 0 to 30 mol/m^3. Therefore the Langmuir number, La ($=C_\infty/\beta$), which is the ratio of the adsorption rate, kC_∞, to the desorption rate, $k\beta$, ranges from 0 to 1.38. The value of Γ is initially set at 0 mol/m^2 all over the interface. The time step size is 0.001 ms for the 0.60 mm bubble and 0.002 ms for the other bubbles.

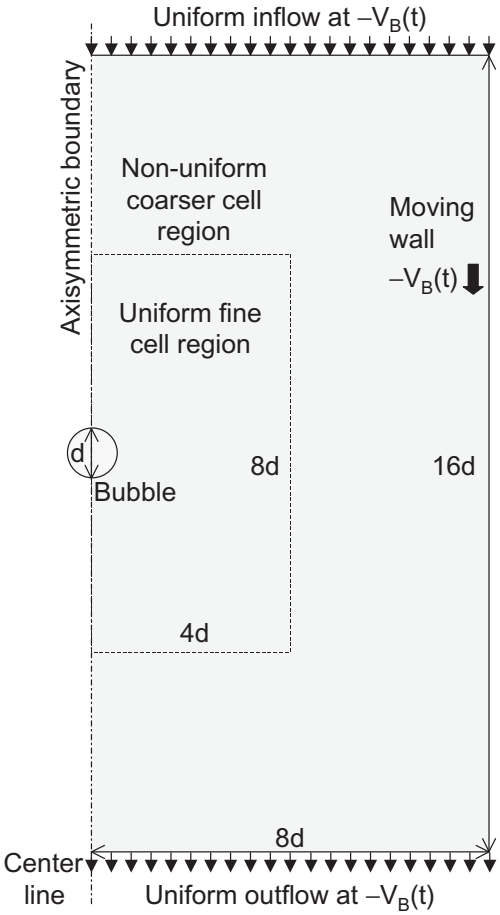

Fig. 1. Computational domain for simulations of single air bubbles in stagnant liquids.

The grid dependency is examined for the intermediate bubble size, i.e., $d = 0.72$ mm and $C_\infty = 30\ \mathrm{mol/m^3}$. The number of cells assigned to the bubble diameter is increased up to 72, while the domain size is fixed. The change in the bubble terminal velocity with the increase in the spatial resolution is less than 0.6%.

Predicted distribution of the dimensionless surface concentration Γ^* for $d = 0.72$ mm at $C_\infty = 30\ \mathrm{mol/m^3}$ is shown in Fig. 2a, where Γ^* is defined by $\Gamma^* = \Gamma/\Gamma_{\max}$. The Hatta number defined by $\mathrm{Ha} = kC_\infty d/V_T$ is 1.38, which means that the adsorption velocity is faster than the bubble rising velocity. Due to this, the surfactant covers the whole surface. The Γ^* takes the lowest value at the bubble nose and high values in the bottom region due to the advection of Γ towards the rear. Since the surfactant reduces the surface tension, σ decreases from the nose to rear as shown in Fig. 2b. The gradient of σ is large in the upper half of the bubble, whereas it is very small in the lower half. The strong Marangoni force, $(\nabla_S\sigma)\delta(\phi)$, therefore, appears in the upper half as shown in Fig. 2c. Since the Marangoni number, Ma ($=RGT\Gamma_{\max}/\mu V_T$), is 181, the Marangoni force should have a large impact on the bubble motion.

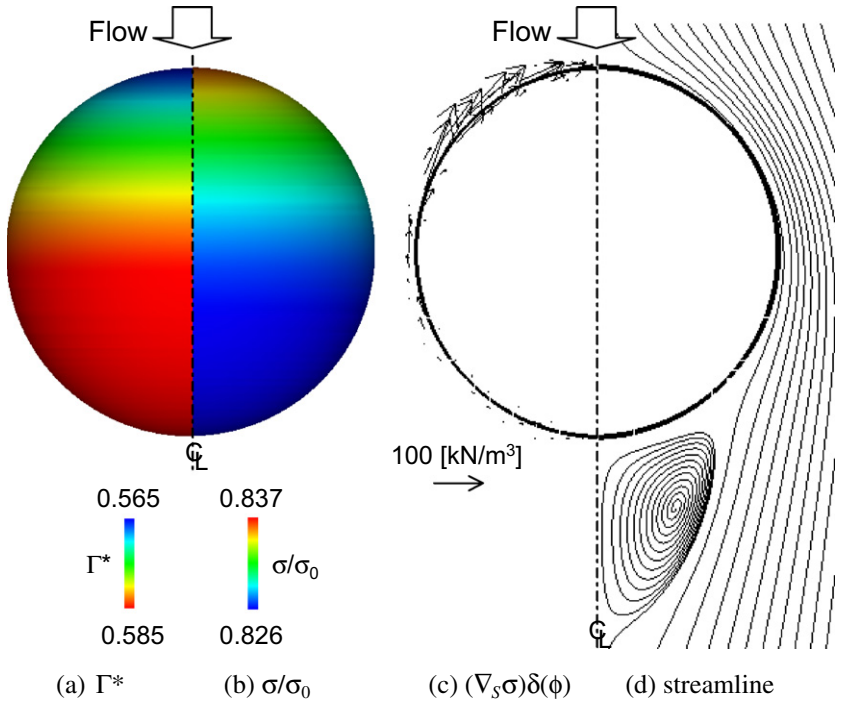

Fig. 2. Distributions of Γ, σ and Marangoni force, and streamline (d = 0.72 mm, C_∞ = 30 mol/m^3).

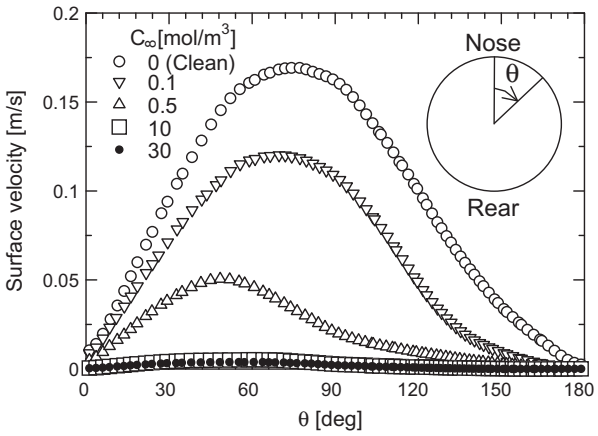

Fig. 3. Surface velocities of 0.72 mm bubbles.

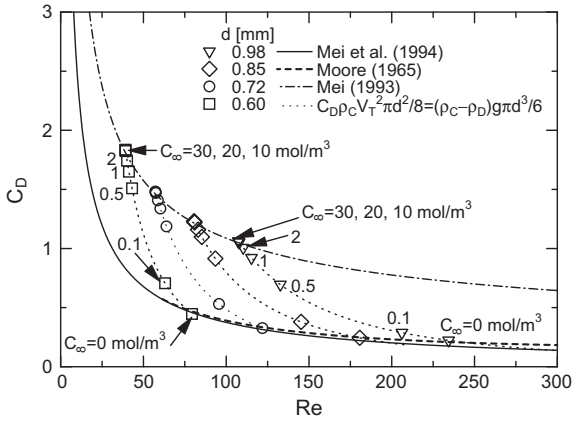

Fig. 4. Effects of surfactant on drag coefficients of air bubbles in water.

Fig. 3 shows the surface velocities of 0.72 mm bubbles at different C_∞. The surface velocity decreases with increasing C_∞ and the surface is almost immobile for $C_\infty \geqslant 10$ mol/m^3. Fig. 2d shows streamlines about the contaminated bubble of C_∞ = 30 mol/m^3. The internal circulation is attenuated and the separation of the flow takes place. The bubble Reynolds number, $\mathrm{Re} = \rho_L V_T d/\mu_L$, of this bubble is 57.2. The computed angle, θ_S, from the bubble nose to the separation point from the bubble surface is 137°. The empirical correlation of θ_S for a solid sphere proposed by Clift et al. (1978), $\theta_S = 180 - 42.5[\ln(\mathrm{Re}/20)]^{0.483}$, gives 136°. This agreement indicates that the flow about the contaminated bubble is similar to that about a solid sphere.

Predicted drag coefficients, C_D, are plotted in Fig. 4. The broken and solid lines are drawn using the model for distorted clean bubbles proposed by Moore (1965)

$$C_D = \frac{48G}{\mathrm{Re}}\left[1 + \frac{H}{\mathrm{Re}^{1/2}}\right] \tag{32}$$

and the model for spherical clean bubbles proposed by Mei et al. (1994)

$$C_D = \frac{24}{\mathrm{Re}}\left[\frac{2}{3} + \left\{\frac{12}{\mathrm{Re}} + 0.75\left(1 + \frac{3.315}{\mathrm{Re}^{1/2}}\right)\right\}^{-1}\right] \tag{33}$$

respectively, where G and H are functions of the aspect ratio of a bubble. The C_D at C_∞ = 0 mol/m^3 agrees well with the Moore's model, which indicates that the effect of slight shape deformation on C_D at these intermediate and high Reynolds numbers is well predicted. The dash-dotted line in the figure is the following drag correlation for solid particles (Mei, 1993):

$$C_D = \frac{24}{\mathrm{Re}}(1 + 0.1935Re^{0.6305}) \tag{34}$$

The predicted C_D approaches to Eq. (34) as the surfactant concentration increases. These results agree with the well-known experimental fact for the Marangoni effect on small bubbles, and therefore, the proposed method can be used for the investigation of the bubble dynamics in the presence of surfactant.

Table 1
Drag coefficients, C_D, of contaminated bubbles compared with those of solid particles at the same Re.

	Arithmetic mean $\mu = \mu_C H_\varepsilon + \mu_D(1 - H_\varepsilon)$			Harmonic mean $\mu^{-1} = \mu_C^{-1} H_\varepsilon + \mu_D^{-1}(1 - H_\varepsilon)$		
C_∞ (mol/m^3)	Re	C_D	C_{Dsolid}*	Re	C_D	C_{Dsolid}*
10	57.5	1.47	1.46	66.7	1.09	1.34
20	57.3	1.48	1.46	66.4	1.10	1.35
30	57.2	1.48	1.46	66.1	1.11	1.35

* Evaluated with Eq. (34).

Let us then briefly discuss the effect of an averaging scheme for viscosity. Table 1 shows a comparison between the predicted drag coefficients of 0.72 mm bubbles at their fully-contaminated conditions and those obtained using the harmonic mean for the viscosity. The drag coefficient with the harmonic mean does not reach the value of the solid particle. This is because the harmonic mean makes the tangential viscous stress at the bubble surface continuous, and therefore, the tangential component of the momentum jump condition with the Marangoni force is not satisfied.

4.2. Taylor bubbles rising through stagnant water in vertical pipes

Effects of surfactant on the terminal velocities and shapes of contaminated Taylor bubbles in low Morton number systems are investigated using the proposed interface tracking method. Fluid properties used are those for an air–water system at room temperature and atmospheric pressure. Therefore the Morton number is low, i.e., $M = 2.5 \times 10^{-11}$. The Eötvös number tested ranges from 4.8 to 120 ($6.0 \leqslant D \leqslant 30$ mm, where D is the pipe diameter). The surfactant properties are the same as those used in the previous simulation and $C_\infty = 30$ mol/m^3.

The dimensions of the computational domain are $0.5D$ and $8D$ in the r and z directions, respectively. Uniform computational cells are used. The cell width is $D/96$, whereas a higher resolution, $D/192$, is used only for the bubble at $Eo_D = 4.8$ to resolve a thin liquid film between the bubble and the pipe wall. The time step size Δt is varied from 0.001 ms to 0.1 ms for assuring numerical stability. The top, bottom and right boundaries are uniform inflow at constant speed, continuous outflow and no-slip wall moving downward at the inflow speed, respectively. The left boundary is the axis of symmetry. A finer cell width of $D/144$ is tested for the cases of $Eo_D = 8.6$ and 84 and $C_\infty = 30$ mol/m^3. For both cases, the changes in the bubble terminal velocity with the increase of spatial resolution are less than 0.3%.

Bubble shapes and terminal velocities at $Eo_D = 120$ and 4.8 are shown in Fig. 5. The Hatta numbers defined by using the pipe diameter are 24 and 66, respectively. The shapes of the clean and contaminated bubbles at $Eo_D = 120$ are the same in the top and side regions. The terminal velocities are also the same. Hence there are no substantial effects of surfactant on V_T and front and side shapes at high Eo_D and low M. On the other hand, at lower Eo_D, V_T of the contaminated bubble is twice as large as that of the clean bubble and shapes are slightly different.

Distributions of Γ^*, σ and $(\nabla_S\sigma)\delta_\varepsilon(\phi)$ and streamlines at $Eo_D = 120$ and 4.8 are shown in Figs. 6 and 7. All the surface is covered by surfactant in both cases since their Hatta numbers are high. The surface tension reduction, therefore, takes place all over the interface. The gradient of σ is small except the bottom region. Hence the Marangoni force acts only on that region. The Γ^* at $Eo_D = 120$ takes the maximum value at the junction between the wake and the downward film flow between the bubble and the pipe wall, whereas, at $Eo_D = 4.8$, Γ^* is high in the whole bottom region and no separation occurs. These indicate that the Γ distribution in the bottom part of the bubble strongly depends on the wake structure. At $Eo_D = 4.8$, the Marangoni number is very high, Ma = 1042. The surface immobilization, however, is not significant at the bubble surface in the bottom since the σ gradient is not so large.

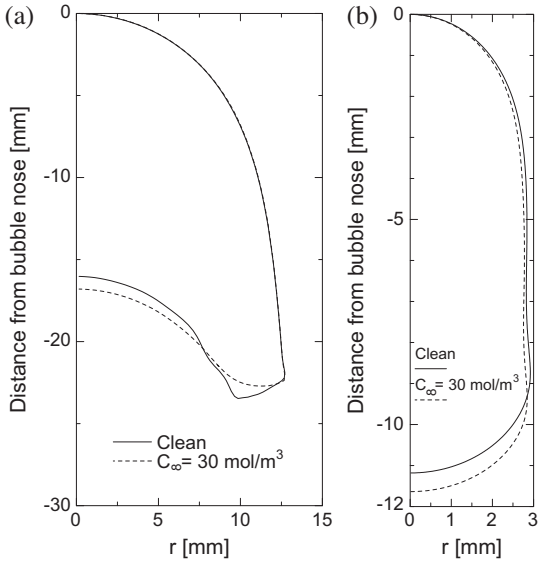

V_T (clean) [m/s]	0.187	0.0069
V_T (contaminated) [m/s]	0.187	0.0138

Fig. 5. Bubble shapes (a) $Eo_D = 120$ ($d/D = 0.8$) (b) $Eo_D = 4.8$ ($d/D = 1.27$).

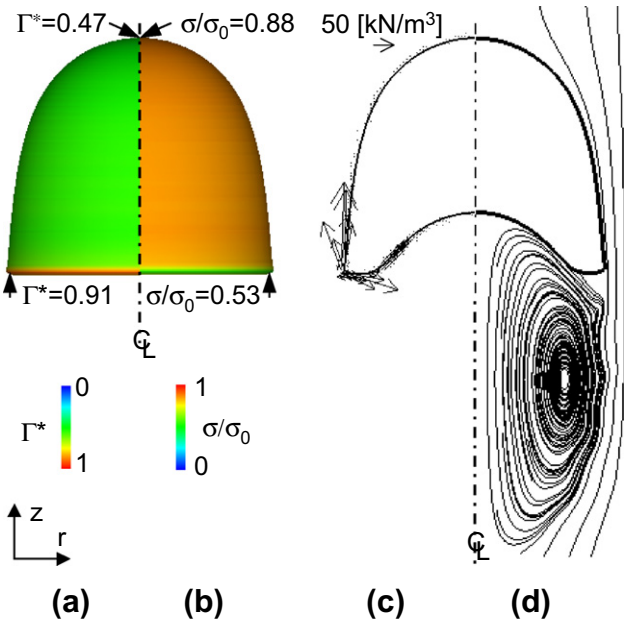

Fig. 6. Distributions of (a) Γ^*, (b) $\sigma(\Gamma)$ and Marangoni force $(\nabla_S\sigma)\delta_\varepsilon(\phi)$, and (d) streamline at $Eo_D = 120$.

Predicted Froude numbers of the clean and contaminated Taylor bubbles are shown in Fig. 8. Measured data of clean bubbles (White and Beardmore, 1962) are also plotted for comparison. The predictions of the clean bubbles agree with the measured data. This comparison clearly shows that the surfactant increases Fr only at low Eo_D numbers. To make clear the contribution of the Marangoni force to the decrease in Fr, simulations of the Taylor bubbles

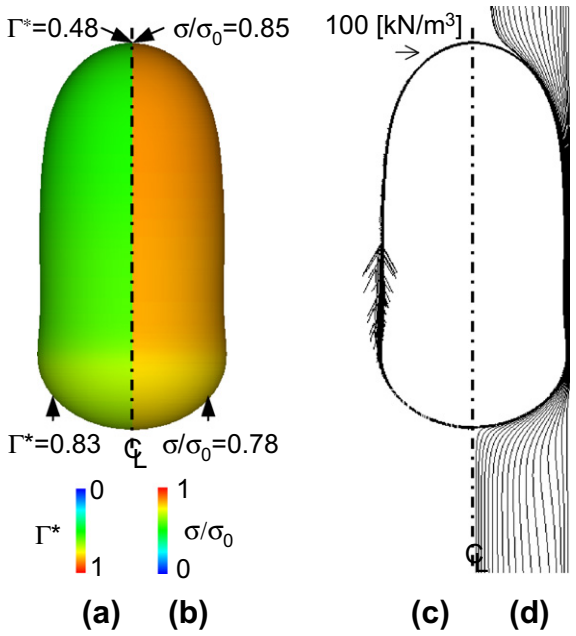

Fig. 7. Distributions of (a) Γ^*, (b) $\sigma(\Gamma^*)$ and Marangoni force $(\nabla_S\sigma)\delta_\varepsilon(\phi)$, and (d) streamline at $Eo_D = 4.8$.

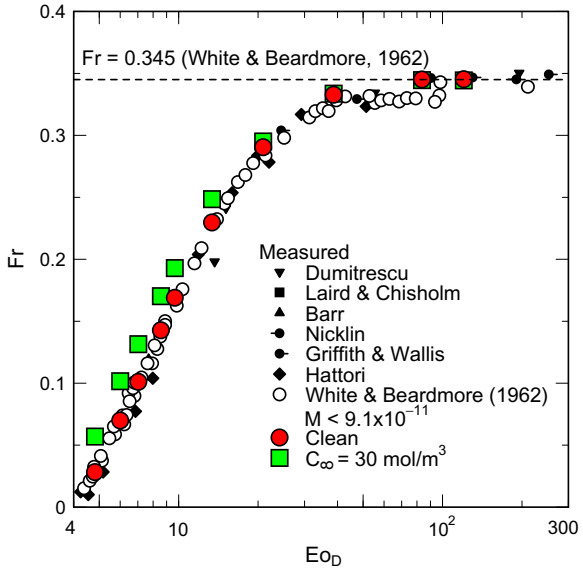

Fig. 8. Froude numbers of clean and contaminated Taylor bubbles.

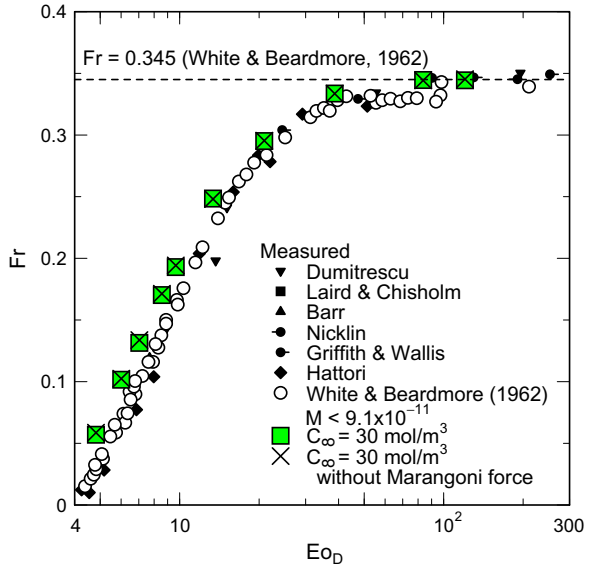

Fig. 9. Effect of Marangoni force on Fr.

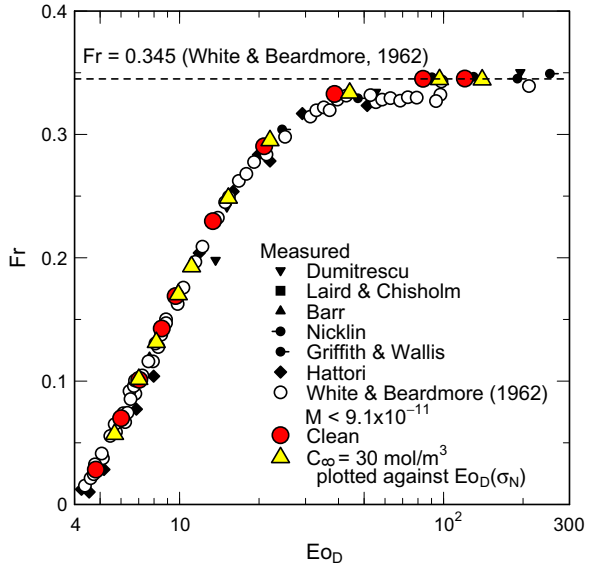

Fig. 10. Froude numbers of contaminated Taylor bubbles correlated in terms of Eo_D using surface tension at the bubble nose, σ_N.

without the Marangoni force are also carried out. The predicted Fr is plotted with cross symbols in Fig. 9. The difference in Fr between the simulations with and without $\nabla_S\sigma$ is negligibly small. Hence the Marangoni force does not have much influence on the velocity reduction. According to Tomiyama (2004) and Funada et al. (2005), Fr of a clean Taylor bubble can be related to the local aspect ratio or mean curvature at the bubble nose. It is, therefore, expected that the surface tension in the nose region plays a dominant role in Fr of a contaminated Taylor bubble. The Froude numbers of contaminated bubbles are, therefore, re-plotted against Eo_D using σ_N, which is the surface tension at the bubble nose, in Fig. 10. The Froude numbers with the modified Eo_D agree well with those of the clean bubbles. Fig. 11 shows the radius of curvature, R_N, at the bubble nose scaled by the pipe radius, R, against Fr. The dependencies of Fr on R_N/R for the clean and contaminated bubbles are in good agreement, which also supports that Fr can be modeled in terms of the surface condition in the nose region not only for the clean bubble but also for the contaminated bubble. The surface tension in the nose region is, therefore, a key parameter in modeling Fr of contaminated Taylor bubbles.

Fig. 12 shows predicted Froude numbers of Taylor bubbles in 8.5 mm pipe ($Eo_D(\sigma_0) = 9.7$) at various surfactant concentrations, i.e., $10 \leqslant C_\infty \leqslant 2750$ mol/m^3. For this range of C_∞, *La* ranges from 0.46 to 127. The fluid properties of the air–water system are used even at very high 1-pentanol concentrations since the simulations are carried out just to examine whether or not the above discussion on Fr holds even at high concentrations. The Froude number monotonously increases with C_∞ and the modified Eötvös number $Eo_D(\sigma_N)$ does work well, which indicates that the above discussion, i.e., the terminal velocity of the Taylor bubble is governed by the

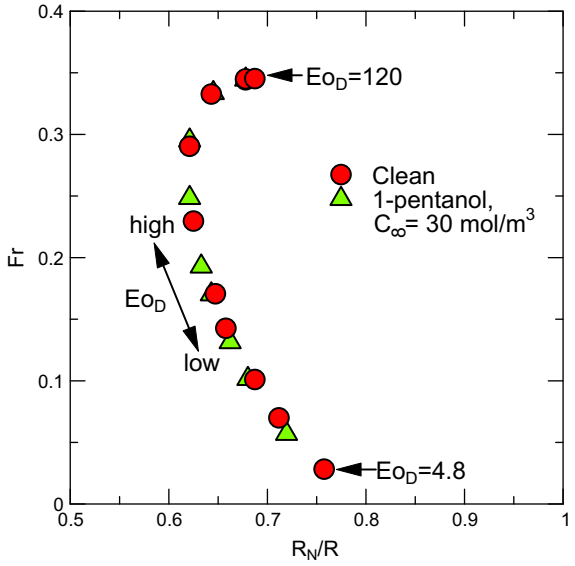

Fig. 11. Radius of curvature at bubble nose.

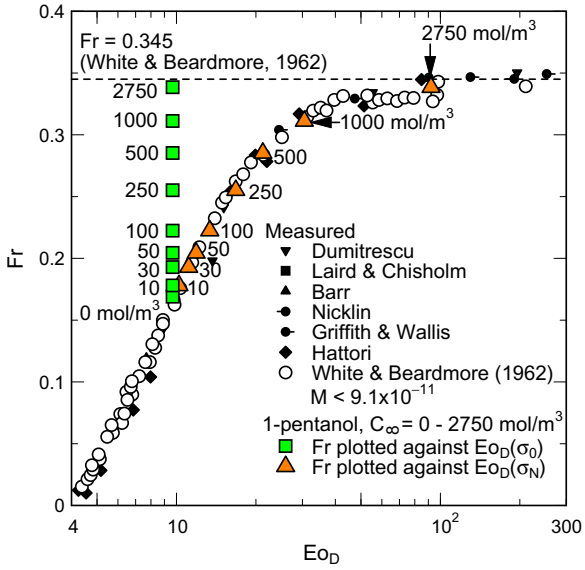

Fig. 12. Froude numbers of contaminated Taylor bubbles at $Eo_D(\sigma_0) = 9.7$ plotted against Eo_D with σ_N.

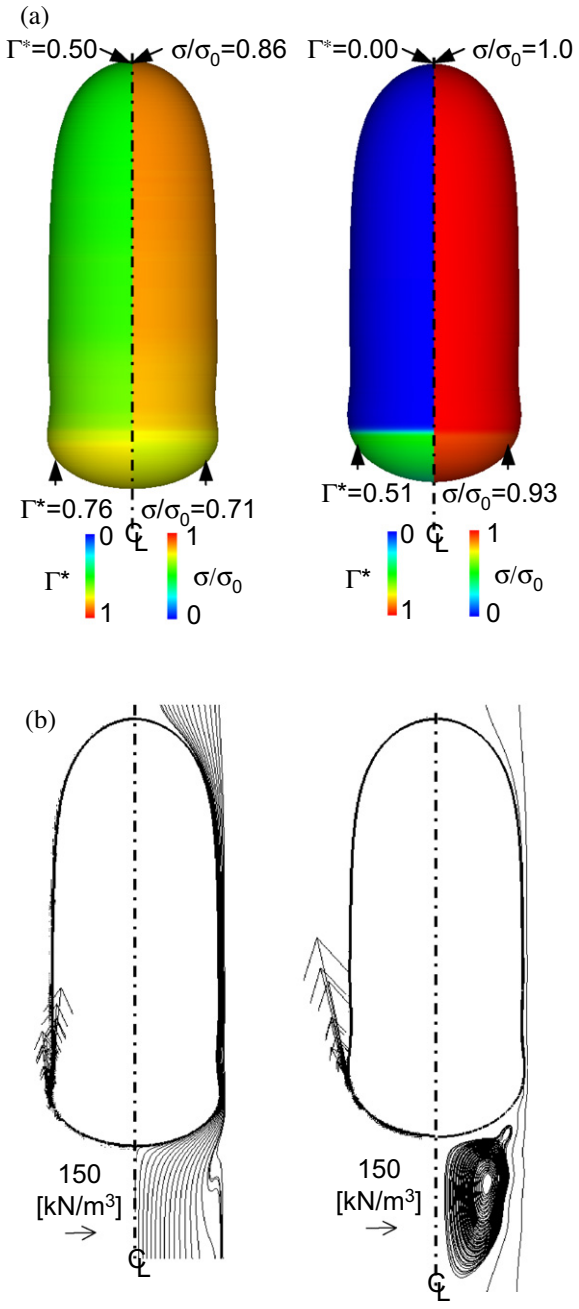

Fig. 13. Comparison between surfactant effects for different surfactants (left column: 1-pentanol at $C_\infty = 30$ mol/m^3, right: Triton X-100 at $C_\infty = 3.2 \times 10^{-3}$ mol/m^3) (a) Γ and σ distributions (b) Streamline and Marangoni force.

surface condition near the bubble nose, also holds at high concentrations.

Then the surfactant properties of Triton X-100 are used to investigate the effect of adsorption and desorption properties. The coefficients, k, β, and Γ_{max}, of Triton X-100 are 50 m^3/mol s, 6.6×10^{-4} mol/m^3 and 2.9×10^{-6} mol/m^2, respectively (Takagi et al., 2003). The bulk diffusion coefficient D_C is 3.0×10^{-10} m^2/s (Leaist, 1991). It is assumed that $D_C = D_S$. The bulk concentration, C_∞, is determined as a value satisfying $[\sigma(C_\infty)]_{1\text{-pentanol}} = [\sigma(C_\infty)]_{\text{TritonX-100}}$, i.e., for Triton X-100, $C_\infty = 3.2 \times 10^{-3}$ mol/m^3, which is much lower than the critical micelle concentration, 0.24 mol/m^3. The Langmuir number is 4.8, and therefore, the adsorption is much more dominant than the desorption compared with 1-pentanol.

Taylor bubbles contaminated with 1-pentanol and Triton X-100 at $Eo_D = 7.1$ are compared in Fig. 13. The surfactant distribution is by far different, i.e., Triton X-100 adsorbs only in the bottom region and the nose and side regions are almost free from surfactant. The cause of this distribution is as follows. Surfactants adsorbed in the nose and side regions are immediately advected toward the bottom region since the Hatta number is very low, i.e., Ha = 0.043 (Ha = 32 for 1-pentanol). Then the surfactant accumulates in the bottom since the adsorption is superior to the desorption. The steep gradient of σ in the bottom region causes the large Marangoni force, which immobilizes the bottom surface and separates the flow at this point. This comparison of surfactant distributions between 1-pentanol and Triton X-100 indicates that the Hatta number is a primary parameter determining the degree of contamination in the nose region.

For $4.8 \leqslant Eo_D \leqslant 120$, Ha ranges from 0.13 to 0.026, and the surfaces near the bubble noses are almost clean for all the cases. The

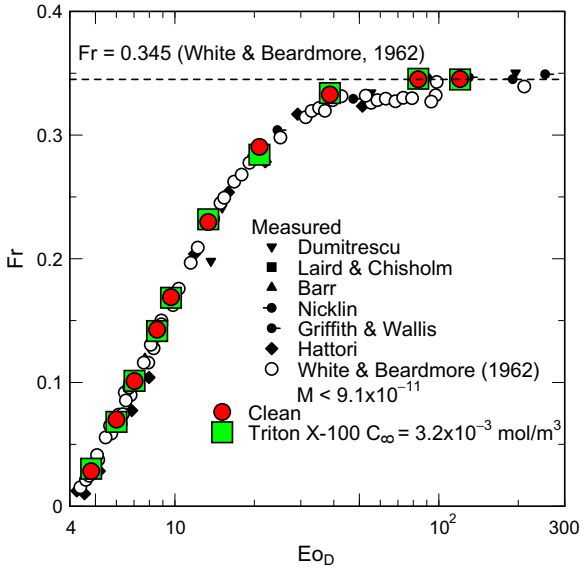

Fig. 14. Froude numbers of Taylor bubbles contaminated with Triton X-100. The surface tension σ_0 is used for Eo_D.

change in Froude number due to the presence of surfactant is very small at all the Eo_D numbers as shown in Fig. 14.

For both surfactants, the Froude numbers of contaminated bubbles can be evaluated by making use of available Fr correlations for clean bubbles, provided that the surface condition in the nose region is known. It should, however, be noted that in all the cases considered in this study the Marangoni force in the nose region is negligibly small, in other words, the surface tension is nearly constant near the bubble nose. If the Marangoni force is large in the nose region, its surface immobilization effect should be accounted for in Fr.

5. Conclusion

An interface tracking method for predicting fluid interfaces contaminated with soluble surfactant was proposed. The method is based on a carefully-determined combination of available schemes such as the level set method for interface tracking, the ghost fluid method for computing the normal component of surface tension force, the CSF model for computing the tangential component, an approximation method for computing bulk concentration of surfactant, the extrapolation method for computing surface gradient, and the Frumkin–Levich model for the adsorption–desorption kinetics.

Small air bubbles rising through stagnant water contaminated with 1-pentanol were simulated for validation of the proposed method. Taylor bubbles rising through vertical pipes filled with contaminated water at a low Morton number were then simulated. The Morton number was 2.5×10^{-11} and the Eötvös number ranged from 4.8 to 120. Various bulk concentrations of 1-pentanol were tested. Effects of surfactant properties were discussed by comparing the surfactant distributions and the Froude numbers for 1-pentanol and Triton X-100. The main conclusions obtained are as follows:

(1) The surface immobilization and the increase in drag of small bubbles due to the presence of surfactant, i.e., the Marangoni effects, are well predicted using the developed method.
(2) When the Marangoni force is present, the arithmetic mean should be used for the viscosity since the harmonic mean causes a large error in the tangential component of the momentum jump condition.
(3) The reduction of surface tension near the bubble nose is the cause of the increase in terminal velocity of a Taylor bubble at a low Eötvös number.
(4) The surfactant does not affect the Froude numbers of high Eötvös number Taylor bubbles since the Froude number is independent of surface tension at high Eötvös numbers.
(5) The Froude number of a low Morton number Taylor bubble can be evaluated by making use of available correlations for the clean Taylor bubble, provided that the surface tension near the bubble nose is known and the Marangoni effect in the nose region is negligible.
(6) The Hatta number is a primary factor governing the degree of contamination in the bubble nose region of a Taylor bubble.

Acknowledgments

This work has been supported by the Hyogo Science and Technology Association and the Japan Society for the Promotion of Science (Grant-in-aid for scientific research (B), No. 21360084).

References

Alke, A., Bothe, D., 2009. 3D numerical modeling of soluble surfactant at fluidic interfaces based on the volume-of fluid method. Fluid Dynam. Mater. Process. 1 (1), 1–30.
Almatroushi, E., Borhan, A., 2004. Surfactant effect on the buoyancy-driven motion of bubbles and drops in a tube. Ann. N.Y. Acad. Sci. 1027, 330–341.
Aslam, T.D., 2003. A partial differential equation approach to multidimensional extrapolation. J. Comput. Phys. 193, 349–355.
Aybers, N.M., Tapucu, A., 1969. Studies on the drag and shape of gas bubbles rising through a stagnant fluid. Wärme Stoffübertrag 2, 171–177.
Brackbill, J.U., Kothe, D.B., Zemach, C., 1992. A continuum method for modeling surface tension. J. Comput. Phys. 100 (2), 335–354.
Chang, Y.C., Hou, T.Y., Merriman, B., Osher, S., 1996. A level set formulation of Eulerian interface capturing methods for incompressible fluid flows. J. Comput. Phys. 124, 449–464.
Clift, R., Grace, J.R., Weber, M.E., 1978. Bubbles, Drops, and Particles. Academic Press.
Cuenot, B., Magnaudet, J., Spennato, B., 1997. The effects of slightly soluble surfactants on the flow around a spherical bubble. J. Fluid Mech. 339, 25–53.
Enright, D., Fedkiw, R., Ferziger, J., Mitchell, I., 2002. A hybrid particle level set method for improved interface capturing. J. Comput. Phys. 183, 83–116.
Fedkiw, R.P., Aslam, T., Merriman, B., Osher, S., 1999. A non-oscillatory Eulerian approach to interfaces in multimaterial flows (the ghost fluid method). J. Comput. Phys. 152, 457–492.
Frumkin, A., Levich, V.G., 1947. On surfactants and interfacial motion. Zh. Fiz. Khim. 21, 1183–1204 (in Russian).
Fukuta, M., Takagi, S., Matsumonoto, Y., 2008. Numerical study on the shear-induced lift force acting on a spherical bubble in aqueous surfactant solutions. Phys. Fluids 20, 040704.
Funada, F., Joseph, D.D., Maehara, T., Yamashita, S., 2005. Ellipsoidal model of the rise of a Taylor bubble in a round tube. Int. J. Multiph. Flow 31, 473–491.
Hayashi, K., Kurimoto, R., Tomiyama, A., 2010. Dimensional analysis of terminal velocity of a Taylor bubble in a vertical pipe. Multiph. Sci. Technol. 22 (3), 197–210.
James, A.J., Lowengrub, J., 2004. A surfactant-conserving volume-of-fluid method for interfacial flows with insoluble surfactant. J. Comput. Phys. 201, 685–722.
Kang, M., Fedkiw, R.P., Liu, X.-D., 2000. A boundary condition capturing method for multiphase incompressible flow. J. Sci. Comput. 15 (3), 323–360.
Leaist, D.G., 1991. A moving-boundary technique for the measurement of diffusion in liquids: triton X-100 in Water. J. Solution Chem. 20 (2), 187–197.
LeVeque, R., Li, Z., 1994. The immersed interface method for elliptic equations with discontinuous coefficients and singular sources. SIAM J. Numer. Anal. 31, 1019–1044.
Levich, V.G., 1962. Physicochemical Hydrodynamics. Prentice Hall.
Liao, Y., McLaughlin, J.B., 2000. Bubble motion in aqueous surfactant solutions. J. Colloid Interf. Sci. 224, 297–310.
Mei, R., 1993. History force on a sphere due to a step change in the free-stream velocity. Int. J. Multiph. Flow 19, 509–525.
Mei, R., Klausner, J.F., Lawrence, C.J., 1994. A note on the history force on a spherical bubble at finite Reynolds number. Phys. Fluids A 6 (1), 418–420.
Meier, M., 2000. Towards a DNS of Multiphase Flow. Technical Report No. LKT-01-00, Laboratorium fur Kerntechnik Institutfu fur Energietechnik, ETH Zurich.
Moore, D.W., 1965. The velocity of rise of distorted gas bubbles in a liquid of small viscosity. J. Fluid Mech. 23, 749–766.
Muradoglu, M., Tryggvason, G., 2008. A front-tracking method for computation of interfacial flows with soluble surfactants. J. Comput. Phys. 227, 2238–2262.
Prosperetti, A., 2002. In: Rein, M. (Ed.), Drop-Surface Interactions. Springer.

Stone, H.A., 1990. A simple derivation of the time-dependent convective-diffusion equation for surfactant transport along a deforming interface. Phys. Fluids A 2 (1), 111–112.

Sussman, M., Smereka, P., Osher, S., 1994. A level set approach for computing solutions to incompressible two-phase flow. J. Comput. Phys. 114 (1), 146–159.

Sussman, M., Fatemi, E., Smereka, P., Osher, S., 1998. An improved level set method for incompressible two-phase flows. Comput. Fluids 27, 663–680.

Takagi, S., Uda, T., Watanabe, Y., Matsumoto, Y., 2003. Behavior of a rising bubble in water with surfactant dissolution (1st report, steady behavior). Trans. Jpn. Soc. Mech. Eng. 69 (686), 2192–2199 (in Japanese).

Takagi, S., Ogasawara, T., Fukuta, M., Matsumoto, Y., 2009. Surfactant effect on the bubble motions and bubbly flow structures in a vertical channel. Fluid Dyn. Res. 41, 065003 (17 pages).

Takewaki, H., Yabe, T., 1987. The cubic-interpolated pseudo particle (CIP) method: application to nonlinear and multi-dimensional hyperbolic equations. J. Comput. Phys. 70, 355–372.

Tomiyama, A., 2004. Drag, lift and virtual mass forces acting on a single bubble. In: Proceedings of the 3rd International Symposium on Two-Phase Flow Modelling and Experimentation, CD-ROM. Pisa, p. 10.

Tryggvason, G., Scardovelli, R., Zaleski, S., 2011. Direct Numerical Simulations of Gas Liquid Multiphase Flows. Cambridge.

Tukovic, Z., Jasak, H., 2008. Simulation of free-rising bubble with soluble surfactant using moving mesh finite volume/area method. In: Proceedings of the 6th International Conference on CFD in Oil & Gas, Metallurgical and Process Industries, CFD08-09. Norway, p. 11.

Viana, F., Pardo, R., Yanez, R., Trallero, J.L., Joseph, D., 2003. Universal correlation for the rise velocity of long gas bubbles in round pipes. J. Fluid Mech. 494, 379–398.

Wallis, G.B., 1969. One-Dimensional Two-Phase Flow. McGraw-Hill, New York.

Wang, J., Lu, P., Wang, Z., Chao, Y., Mao, Z.-S., 2008. Numerical simulation of unsteady mass transfer by the level set method. Chem. Eng. Sci. 63, 3141–3151.

White, E.T., Beardmore, R.H., 1962. The velocity of rise of single cylindrical air bubbles through liquids contained in vertical tubes. Chem. Eng. Sci. 17, 351–361.

Xu, J.-J., Zhao, H.-K., 2003. An Eulerian formulation for solving partial differential equations along moving interface. J. Sci. Comput. 19, 573–594.

Xu, J.-J., Li, Z., Lowengrub, J., Zhao, H., 2006. A level-set method for interfacial flows with surfactant. J. Comput. Phys. 212, 590–616.